Pnictogen-Centered Cascade Exchangers for Thiol-Mediated Uptake: As(III)-, Sb(III)-, and Bi(III)-Expanded Cyclic Disulfides as Inhibitors of Cytosolic Delivery and Viral Entry

Lim, Bumhee; Kato, Takehiro; Besnard, Céline; Poblador Bahamonde, Amalia Isabel; Sakai, Naomi; Matile, Stefan

How to cite

LIM, Bumhee et al. Pnictogen-Centered Cascade Exchangers for Thiol-Mediated Uptake: As(III)-, Sb(III)-, and Bi(III)-Expanded Cyclic Disulfides as Inhibitors of Cytosolic Delivery and Viral Entry. In: JACS Au, 2022, vol. 2, n° 5, p. 1105–1114. doi: 10.1021/jacsau.2c00017

This publication URL: https://archive-ouverte.unige.ch/unige:161348

Publication DOI: 10.1021/jacsau.2c00017

JACS Au
AN OPEN ACCESS JOURNAL OF THE AMERICAN CHEMICAL SOCIETY

pubs.acs.org/jacsau

Article

Pnictogen-Centered Cascade Exchangers for Thiol-Mediated Uptake: As(III)-, Sb(III)-, and Bi(III)-Expanded Cyclic Disulfides as Inhibitors of Cytosolic Delivery and Viral Entry

Bumhee Lim, Takehiro Kato, Celine Besnard, Amalia I. Poblador Bahamonde, Naomi Sakai, and Stefan Matile*

Cite This: *JACS Au* 2022, 2, 1105−1114

Read Online

ACCESS | Metrics & More | Article Recommendations | Supporting Information

ABSTRACT: Dynamic covalent exchange cascades with cellular thiols are of interest to deliver substrates to the cytosol and to inhibit the entry of viruses. The best transporters and inhibitors known today are cyclic cascade exchangers (CAXs), producing a new exchanger with every exchange, mostly cyclic oligochalcogenides, particularly disulfides. The objective of this study was to expand the dynamic covalent chalcogen exchange cascades in thiol-mediated uptake by inserting pnictogen relays. A family of pnictogen-expanded cyclic disulfides covering As(III), Sb(III), and Bi(III) is introduced. Their ability to inhibit thiol-mediated cytosolic delivery is explored with fluorescently labeled CAXs as transporters. The promise of inhibiting viral entry is assessed with SARS-CoV-2 lentiviral vectors. Oxygen-bridged seven-membered 1,3,2-dithiabismepane rings are identified as privileged scaffolds. The same holds for six-membered 1,3,2-dithiarsinane rings made from asparagusic acid and *para*-aminophenylarsine oxide, which are inactive or toxic when used alone. These chemically complementary Bi(III) and As(III) cascade exchangers inhibit both thiol-mediated cytosolic delivery and SARS-CoV-2 lentivector uptake at concentrations of 10 μM or lower. Crystal structures, computational models, and exchange kinetics support that lentivector entry inhibition of the contracted dithiarsinane and the expanded dithiabismepane rings coincides with exchange cascades that occur without the release of the pnictogen relay and benefit from noncovalent pnictogen bonds. The identified leads open perspectives regarding drug delivery as well as unorthodox approaches toward dynamic covalent inhibition of cellular entry.

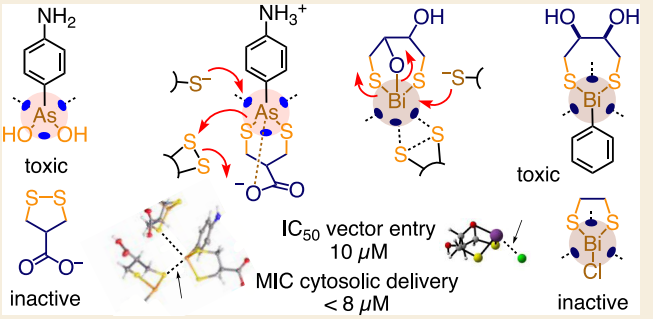

KEYWORDS: *dynamic covalent chemistry, bismuth, arsenic, pnictogen-expanded cyclic disulfides, pnictogen-centered exchange cascades, pnictogen bonds, thiol-mediated uptake, lentivector entry inhibition*

INTRODUCTION

Thiol-mediated uptake is emerging as the method of choice to directly deliver substrates into the cytosol of cells.[1−10] The inhibition of thiol-mediated uptake is of interest because many viruses use the same mechanism to enter cells.[11] Currently unfolding understanding is centered around dynamic covalent exchange cascades with thiols and disulfides from possibly coupled cellular partners (Figure 1B).[1] The receptors known to participate in oligonucleotide phosphorothioate uptake[12−14] and viral entry[1,14−19] provide an impression of the scope and complexity of the network involved. For thiol-mediated cytosolic delivery, cyclic oligochalcogenides **I** such as asparagusic acid **1** have received most attention as dynamic covalent cascade exchangers (CAXs, defined here as exchangers that produce a new, or offer another, exchanger upon exchange; Figure 1A).[1,17] Upon opening by cell surface thiol/ates, they provide a tethered thiol/ate to launch dynamic covalent exchange cascades (Figure 1B). More recently, cyclic oligochalcogenides have been identified as unorthodox candidates to also inhibit viral entry.[11] Here, we introduce pnictogen (Pn)-expanded cascade exchangers (p-CAXs) **II** such as aminophenyl-dithiarsinane **2** and dithiabismepane **3** to integrate pnictogen relays into chalcogen exchange cascades (Figure 1) and show that they inhibit the thiol-mediated cytosolic delivery of fluorescent transporters on the one hand and the entry of SARS-CoV-2 lentivectors on the other.

The combination of pnictogen and chalcogen exchange chemistry is not unusual in medicinal chemistry.[20−29] Arsphenamine, also known as Ehrlich's magic bullet against syphilis, the

Received: January 10, 2022
Revised: March 9, 2022
Accepted: March 10, 2022
Published: March 24, 2022

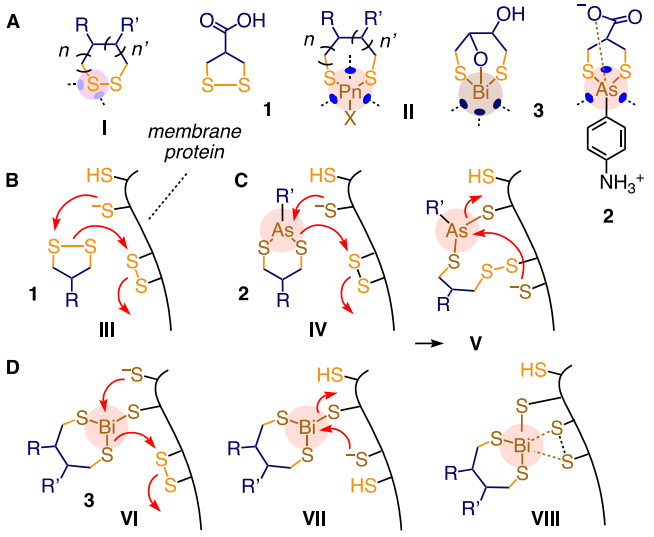

Figure 1. (A) Ring expansion of cyclic disulfides (**I**) with pnictogen relays (**II**), with AspA **1**, phenyl-dithiarsinane **2**, and dithiabismepane **3** as privileged scaffolds (blue ellipses: σ holes; **2** shown as zwitterion with intramolecular As···O pnictogen bond, **3** with intramolecular oxygen ligand). (B) Initiation of dynamic covalent chalcogen exchange cascades between cyclic disulfides and cellular thiols and disulfides. (C) Selected conceivable dynamic covalent chalcogen exchange cascades on pnictogen relay **2** with and (D) pnictogen relay **3** without a permanent substituent include analogous ring-opening cascades (**IV**–**VI**), hopping along thiol/ates (**VII**), and noncovalent pnictogen bonding and hypervalent relays *via* transient or permanent oxidation (**VIII**).

first systematically developed drug, highlights beautifully how the emergence of pnictogen exchanging dynamic covalent networks resembles the adaptive chalcogen exchanging networks operating in thiol-mediated uptake.[24] British Anti-Lewisite (BAL, **4**) operates with the same dynamic covalent chemistry.[25,26] Pnictogen relays are commonly used as antimicrobials and in nanomedicine.[20−23] Ranitidine bismuth citrate, an antiulcer drug, and related bismuth complexes have been shown recently to suppress SARS-CoV-2 replication, possibly acting as helicase or protease inhibitors.[27−29]

While ligand exchange, in general, has a long tradition as an integral part of dynamic covalent chemistry,[30,31] the combination of chalcogen and pnictogen exchange has received little attention. Pioneering work by Johnson and co-workers confirmed operational thiol/ate exchange on arsenic, antimony, and bismuth relays in dynamic covalent macrocyclic architectures.[32,33] In chemical biology, FlAsH probes[34,35] and molecular walkers exchanging along thiol tracks[36] are among the highlights. With regard to cellular uptake, facilitated, glutathione (GSH)-dependent penetration of bismuth has been proposed.[20] The cellular entry of HIV has been inhibited with *para*-aminophenylarsine oxide (aPAO, **5**).[37,38] In addition to this special virology example related to membrane fusion, combined pnictogen and chalcogen exchange chemistry has rarely been considered explicitly for thiol-mediated uptake and its inhibition.

RESULTS AND DISCUSSION

Concepts

The p-CAX **II** appeared attractive for thiol-mediated uptake because of the promise to expand the dynamic covalent chalcogen exchange cascades offered by CAX **I** (**III**, Figure 1B).[1] With a permanent phenyl substituent as in **2**, dynamic covalent exchange with cell surface thiol/ates on pnictogen relays has to proceed by ring opening, which liberates a thiolate that can exchange with cellular disulfides (**IV**, Figure 1C). From the resulting, doubly bridged conjugate, cascades similar to the ones known from **III** can evolve except that the exchanges integrate the specific advantages of pnictogen relays (**V**).

Without permanent phenyl substituent as in **3**, chalcogen exchange with an exofacial thiol/ates can occur also without ring opening (Figure 1D).[36] From the resulting conjugate, ring-opening thiol/ate release for exchange with disulfides (**VI**) is conceivable analogue to **III** and **IV**.[25,26,36] Alternatively, p-CAX **II** could move along thiol/ate tracks (**VII**) in a manner similar to the reported walkers,[36] except that exchange cascades in thiol-mediated uptake, in general, do not occur along rigid tracks but involve significant conformational changes, as exemplified by gp120 in HIV entry,[38] possibly SARS-CoV-2 spike protein,[39] recent surprises with the HaloTag,[40] and so on. Promising new perspectives with pnictogen relays include the involvement of pnictogen bonds[41−43] and hypervalent oxidized intermediates **VIII**, both known to provide new mechanisms in transport and catalysis.[44−50] Already in chalcogen-centered cascades, chalcogen bonding[42,51−55] accounts for exchange without activation energy.[56] The integration of pnictogen bonding increases the strength and versatility (Figure 1A, *vide infra*). Independent of the type of bonding, these pnictogen-thiol interactions could temporarily block exofacial thiols to result in the inhibition of the thiol-mediated uptake.

Synthesis

Inhibitor candidates (**2**−**18**), reporters (**19**−**20**), and transporters (**21**) used in this study were, if not commercially available (**4**, **16**, **17**), prepared in a few steps following or adapting the reported procedures (Figure 2 and Schemes S1−S7). Consistent with the literature,[25,26] and best exemplified by Ehrlich's magic bullet, the spectroscopic data on the structure of the final pnictogen complexes were not always conclusive due to their dynamic nature. In these cases, the drawn structures should be considered as representatives for the entire dynamic covalent network involved. To facilitate reading, p-CAX structures are abbreviated, indicating pnictogen relay, ring size, and substituents, e.g., As-$[6]_{APA}$ for p-CAX **2**, with AP standing for *para*-aminophenyl and A for acid.

Structures

The crystal structure of As-$[6]_{APA}$ **2** showed the *cis*-1,3,2-dithiarsinane in chair conformation **2a** with the carboxylate in equatorial and the phenyl in axial position (Figures 3A and S33). Also most stable in M06-2X/6-311++G**/aug-cc-pVTZ-PP models in water (**2c**, Figures 3E,G and S12−S16), this axial phenyl might indicate a strong anomeric effect that weakens the σ hole and thus pnictogen bonding opposite to the phenyl substituent. In the solid state, dithiarsinanes **2a** dimerized into supramolecular macrocycles stabilized by hydrogen-bonded ion pairs (Figure 3B). These dimers assembled into bilayers with the arsenic relays on their surface (Figure 3C). The closest As(III) contacts are two sulfurs from different chairs. Their position elongating the covalent S−As bonds was consistent with relatively weak intermolecular pnictogen bonds (3.55, 3.71 Å; the sum of the van der Waals radii (VdW) = 3.65 Å, Figure 3D).[57]

Pnictogen bonds in the solid state supported pnictogen-bonding contributions to exchange cascades in thiol-mediated

https://doi.org/10.1021/jacsau.2c00017
JACS Au 2022, 2, 1105−1114

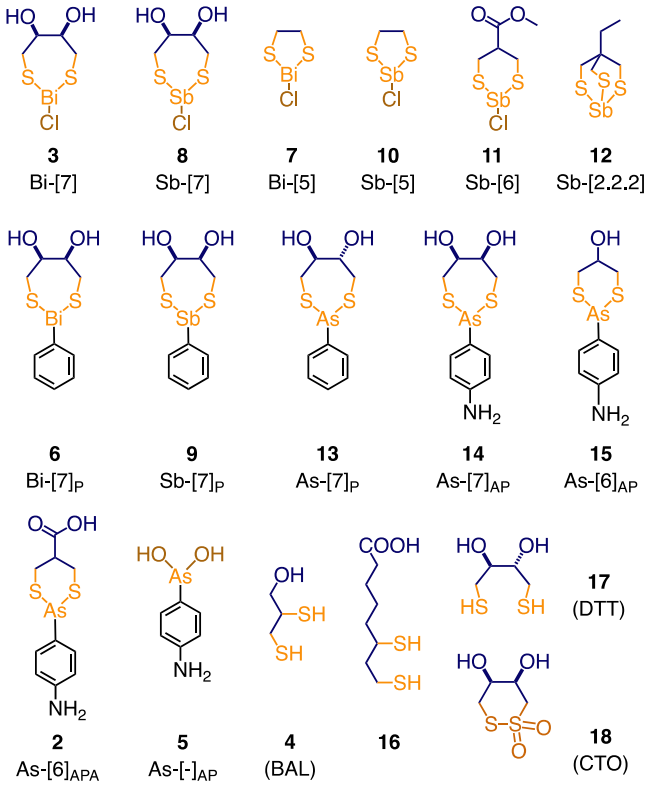

Figure 2. Structures of p-CAXs and dithiols.

uptake (Figure 1, **VIII**). Computed chloride complexes **2c** revealed the existence of pnictogen bonds with nearly perfect angles that increased upon protonation of the arylamine (Figures 3E, 3.49, 3.42 Å; VdW = 3.60 Å). ^{1}H NMR spectroscopy titrations indicated pK_a = 4.0 ± 0.1 for carboxylic acid and pK_a = 8.1 ± 0.1 for ammonium deprotonation (Figures S5 and S6), suggesting that in neutral water, As-[6]$_{APA}$ **2** exists as zwitterion with deepened σ holes for strong pnictogen-bonding contributions.

Zwitterionic bicyclic *trans* boat **2b** and trans chair with two axial substituents were less stable than cis chair **2a** (+6.6, +0.8 kcal mol^{-1}, Figure S13). The As−O distance revealed intramolecular pnictogen bonding in bicyclic **2b** (3.18 Å; VdW = 3.37 Å), which weakened upon deprotonation (3.25 Å) and with *p*-nitro and cyanophenyl (3.20 Å) but not pentafluorophenyl substituents (3.07 Å, Figures 3E and S14).

For the second target Bi-[7] **3**, a known compound,[25] formation of the corresponding bicyclic structure occurs by ligand exchange rather than pnictogen bonding because the permanent phenyl in **2** is replaced by a releasable ligand (Bi-[3.2.1] **3a**: d_c = 2.11 Å, Figure 3F). Pnictogen bonding of water to caged Bi-[3.2.1] **3a** was strong (2.65 Å) and did not weaken upon bond switching by proton transfer (**3b**: 2.67 Å). Pnictogen bonding of chloride was tighter in Bi-[3.2.1] **3a** (2.84 Å, 162.7°, Figure 3G) compared to uncaged **3c** (2.95 Å, 172.7°). Thiolate ligands in Bi-[7] **3b** with powerful (2.71 Å) and less favored hypervalent Bi(V) complexes **3d** with weaker pnictogen bonds (3.25 Å, VdW = 3.59 Å; Figure 3G) were of particular interest as possible intermediates in exchange cascades during thiol-mediated uptake (Figure 1D, **VI**−**VIII**).

Exchange Cascades

Dynamic covalent exchange with p-CAXs was validated in an aqueous buffer solution using the environment-sensitive NBD reporter **19** (Figure 4A). Upon addition of p-CAXs in stoichiometric amounts, fluorescence quenching of varying degrees and rates was observed, indicating the initial formation of Pn complex **22** with two pnictogen-bonding thiols by ligand exchange (Figures 4A,B, S7, and S9). If ligand X is releasable, entropy gains should favor the direct formation of **23** with three thiolate ligands and only one intramolecular pnictogen-bonding thiol. From **22** and **23**, ligand and pnictogen-bonding donor exchange could continue in different ways, including possible relay transfer and polymerization. Similar Pn-generated quenching was absent when the oxidized reporter **20** was used instead of **19** (Figures 4 and S8). Consistent with computational simulations (**3d**, +40.3 kcal mol^{-1} vs **3b**, Figure 3G), experimental support for permanent contributions from hypervalent complex **VIII** could thus not be secured (Figure 1).

Since the extent of quenching should depend on the pnictogens, intensity changes do not report binding strength. However, the difference in rate found within the arsenic series

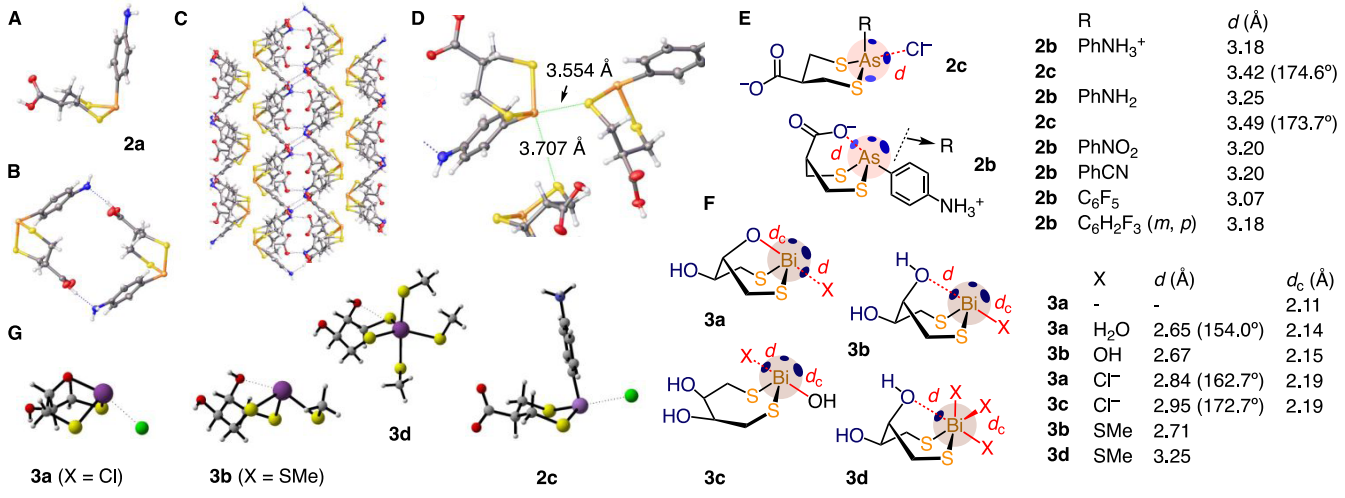

	R	d (Å)
2b	$PhNH_3^+$	3.18
2c		3.42 (174.6°)
2b	$PhNH_2$	3.25
2c		3.49 (173.7°)
2b	$PhNO_2$	3.20
2b	PhCN	3.20
2b	C_6F_5	3.07
2b	$C_6H_2F_3$ (*m*, *p*)	3.18

	X	d (Å)	d_c (Å)
3a	-	-	2.11
3a	H_2O	2.65 (154.0°)	2.14
3b	OH	2.67	2.15
3a	Cl^-	2.84 (162.7°)	2.19
3c	Cl^-	2.95 (172.7°)	2.19
3b	SMe	2.71	
3d	SMe	3.25	

Figure 3. (A−D) Crystal structure of As-[6]$_{APA}$ **2**. (E) Computational models of **2**, with pertinent As−X distances *d* and pnictogen-bond angles, compared to analogues. (F) Same for Bi-[7] **3**, with Bi−X distances *d* compared to covalent bonds d_c. (G) Representative computed structures (d_{VdW}: As−S = 3.65 Å, As−Cl = 3.60 Å, As−O = 3.37 Å, Bi−S = 3.87 Å, Bi−Cl = 3.82 Å, Bi−O = 3.59 Å).

https://doi.org/10.1021/jacsau.2c00017
JACS Au 2022, 2, 1105−1114

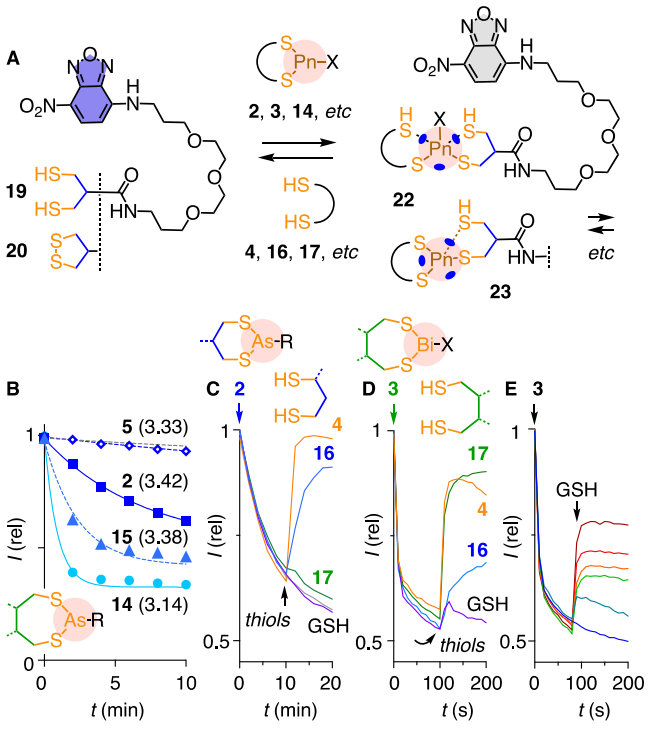

Figure 4. (A) Pnictogen exchange between the reporter **19** and various inhibitors (X = exchangeable ligand or permanent substituent (R in (B, C))). (B) Fluorescence kinetics of **19** (0.1 μM) upon addition of inhibitors at t = 0 (0.1 μM, **2**: filled squares; **5**: empty diamonds; **14**: filled circles; **15**: filled triangles; or none: gray dashed line) in buffer (5 μM TCEP, 10 mM HEPES, 0.1 M NaCl, pH 7.4), λ_{ex} = 465 nm, λ_{em} = 555 nm. In parenthesis: As−Cl distances in computed complexes analogue to **2c**, in Å (from Figures 3E and S12 and S16). (C) Same as (B) upon addition of **2** (0.1 μM) at t = 0, followed by thiols (0.4 μM, **4**: orange; **16**: blue; **17**: green; 0.8 μM GSH: purple; or none: gray) at t = 10 min. (D) as (B) upon addition of **3** (0.1 μM) at t = 0, followed by thiols (0.4 μM, **4**: orange; **16**: blue; **17**: green; 0.8 μM GSH: purple) at t = 100 s. (E) as (B) upon addition of **3** (0.1 μM) at t = 0, followed by GSH (0, 1, 10, 100, 500, 1000 μM) at t = 80 s.

As-$[7]_{AP}$ **14** > As-$[6]_{AP}$ **15** > As-$[6]_{APA}$ **2** > As-$[-]_{AP}$ **5** should reflect the propensity to exchange (Figure 4B). This trend matched the length of the As−Cl pnictogen bonds in chloride complexes analogous to **2c** except for the acyclic As-$[-]_{AP}$ **5** without thiolate ligands, thus suggesting that computational models are predictive (Figures 3E, 4B, and S16). With permanent phenyl substituents necessarily present in the As(III) series and excluding possible oxidation of the pnictogen, the observed rates have to report on ring-opening thiolate exchange to initially afford **22** with two pnictogen bonded thiols. From **22**, exchange of ligands and pnictogen-bond donors can continue up to the possible release of the original dithiol, excluding, however, trithiolates like **23**. The observed rates supported that ring-opening exchange with the contracted 1,3,2-dithiarsinane is slower than with the expanded 1,3,2-dithiarsepane rings (As-$[7]_{AP}$ **14** > As-$[6]_{AP}$ **15**, As-$[6]_{APA}$ **2**), and that γ carboxylates further disfavor ring opening by σ-hole inactivation and ammonium stabilization (As-$[6]_{AP}$ **15** > As-$[6]_{APA}$ **2**; Figure 3E, **2b**).

The reversibility of the process was confirmed by fluorescence recovery upon the addition of excess thiols (**4**, **16**, **17**, or GSH) to complex **22** and the follow-up exchange products (Figures 4C−E and S10). With arsenic complexes, exchange was most efficient with BAL (**4**), followed by lipoic acid (**16**). Consistent with the arsenic detoxification mechanism by BAL,[26] this trend supported that further ring contraction from formal six-membered dithiarsinane to five-membered dithiarsolane rings is favorable. The inability of DTT **17** to displace the reporter from complexes **22** and beyond (Figure 4C, green) confirmed that expansion from arsinanes to seven-membered arsepane rings is not favored. This finding was consistent with the fast exchange of reporter **19** with arsepane **14** (Figure 4B, filled circles). These differences implied that As(III) relays are easily extracted from dithiarsepanes but not from dithiarsinanes, particularly As-$[6]_{APA}$ **2**. The high toxicity of As-$[7]_{AP}$ **14** and As-$[6]_{AP}$ **15** further supported that the lack of toxicity and thus the inhibitory activity of **2** in living cells (*vide infra*) originate from the preservation of the pnictogen relays in the dithiarsinane scaffold, thus validating operational exchange cascades like **IV** and **V** that involve intermediates like **22** (Figures 1C and 4A) and important contributions from pnictogen bonding.

Trends opposite to As(III) were found with Bi(III), i.e, Bi-[7] **3**. This complementarity originated partially from the presence of an exchangeable ligand X, which should undergo direct initial exchange with reporter **19** to trithiolate complex **23** rather than **22**, also for entropic reasons. Contrary to the inactivity with As(III), the dynamic covalent exchange of DTT **17** with the larger Bi(III) complex **23** and beyond became the best. This suggested that ring-expanded seven-membered 1,3,2-dithiabismepane rings were preferred (Figure 4D, green). Even BAL (**4**) was less effective, exchanging fast but continuing to exchange further, maybe polymerize, suggesting that also the contracted five-membered 1,3,2-dithiabismolane rings were inferior to the privileged bismepanes. Also contrary to As(III), exchange with lipoic acid (**16**) into six-membered dithiabismane rings was clearly less favored, thus confirming the preference for bismepanes. As with the contracted As(III) ring in As-$[6]_{APA}$ **2**, these trends supported that the expanded Bi(III) ring in Bi-[7] **3** did not lose the pnictogen relay during biological activity, a conclusion that was consistent with the formation of complexes like **23** during exchange cascades, the inactivity of the contracted Bi-[5] **7**, and the toxicity of the phenyl-substituted Bi-$[7]_{P}$ **6** (*vide infra*).

Operational intramolecular pnictogen bonding was further supported by the inability of glutathione (GSH) to exchange with complexes **22** and **23** under the same conditions (Figure 4C,D, purple). However, higher GSH concentrations as in the cytosol led to exchange with complex **23** and beyond ($EC_{50} \approx 1$ mM, Figure 4E). Compared to GSH, exchange with reduced BSA (bovine serum albumin) was naturally more favored considering the preorganized "vicinal" thiols obtained from disulfide reduction. Since reduced BSA contains 17 vicinal thiols, the obtained EC_{50} values were in the stoichiometric range for both pnictogen complexes ($EC_{50} \approx 6$ nM for reporter **19** with **3**, $EC_{50} \approx 50$ nM for **19** with **2**, Figure S11). Extrapolated to biological systems, these results implied that (1) different pnictogen relays prefer to exchange with differently spaced thiols in proteins and (2) extracellular GSH at μM concentrations would not interfere with this process, while intracellular GSH at mM concentrations could take over pnictogens from the thiols in proteins.

Inhibition of Cytosolic Delivery by Thiol-Mediated Uptake

The fluorescently labeled epidithiodiketopiperazine (ETP) **21** is the transporter of choice to report on the inhibition of thiol-mediated cytosolic delivery because it is very bright, and dynamic covalent chemistry at the disulfide does not

https://doi.org/10.1021/jacsau.2c00017
JACS Au 2022, 2, 1105−1114

significantly affect fluorescence intensity (Figure 5).[11,58] Transporter **21** rapidly penetrates HeLa Kyoto (HK) cells and stains

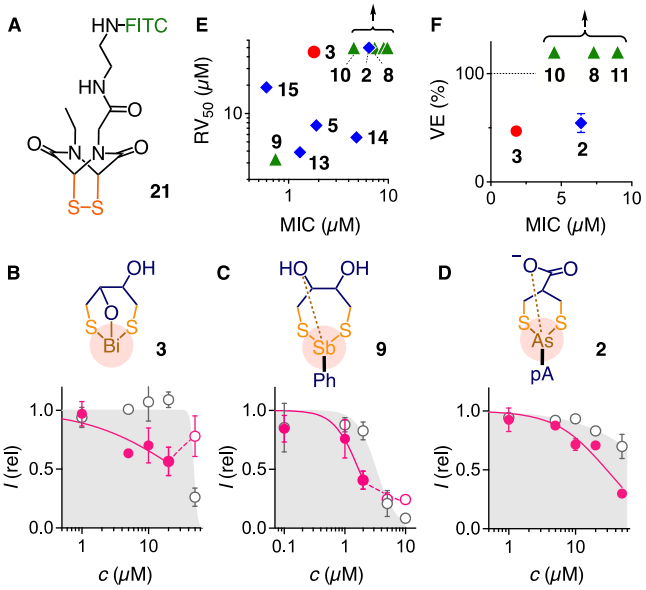

Figure 5. (A) Structure of ETP transporter **21**. (B–D) Representative dose–response curves for the transporter uptake inhibition after incubation of HK cells for 1 h with inhibitors Bi-[7] **3** (B), Sb-$[7]_P$ **9** (C), and As-$[6]_{APA}$ **2** (D), followed by **21** (10 μM). Relative average fluorescence intensity (magenta circles; empty circles: insignificant due to high toxicity) and cell viability (gray empty circles), ± standard deviation (SD), fit with the Hill equation. (E) Comparison of RV_{50} and MIC of pnictogen inhibitors **2**, **3**, **5**, and **8**–**15** for the inhibition of uptake of **21** (red circle: Bi, blue diamonds: As, green triangles: Sb). (F) Comparison of SARS-CoV-2 lentiviral vector entry (VE, %) with 10 μM inhibitor and MIC for the inhibition of the uptake of **21**.

cytosol and nucleus.[58] High-content high-throughput (HCHT) imaging was used to simultaneously determine inhibition and cytotoxicity.[11,59] Inhibitor candidates were added to HK cells in multiwell plates and incubated first for 1 h. In a protocol referred to as pre-incubation, the inhibitors were then removed to avoid exchange with transporter **21**. For co-incubation, inhibitors were kept in the media to allow for exchange also with transporter **21**. After 30 min allowed for transporter **21** to penetrate the cells, Hoechst 33342 and propidium iodide were added to stain the nucleus of all cells and to label necrotic and apoptotic cells, respectively. Their ratio reported relative cell viability (RV, Figures 5B–E and S2–S4 and Tables 1 and S1–S3). Only intact, propidium iodide negative cells were maintained to determine the fluorescence intensity of transporter **21**. This fully automated procedure records uptake independent from toxicity, thus affording correct uptake data even at the onset of toxicity. Uptake inhibition is monitored as decreasing fluorescence with increasing inhibitor concentration and reported as minimal inhibitory concentration (MIC) at 15% inhibition and, if accessible, IC_{50} at 50% inhibition (Figures 5B–E and S2–S4 and Tables 1 and S1–S3).

1,3,2-Dithiabismepane Bi-[7] **3** was envisioned as a lead structure (Figure 3F,G). An MIC = 2 μM and an $IC_{50} \approx 30$ μM were obtained under co-incubation conditions (Figure 5B, red ● and Table 1, entry 2). Both were below a sharp onset of toxicity at ≈50 μM (gray ○). Results with and without inhibitor removal before the addition of transporter **21** were similar, indicating that p-CAX **3** exchanged mostly with cellular thiols

Table 1. Biological Activities of p-CAX Inhibitors[a]

	C[b]	Pn	MIC/IC_{50} (μM)[c]	RV_{50} (μM)[d]	vector entry (%)[e]	cell viability (%)[f]
1	**2**	As-$[6]_{APA}$	6/29	>50	54	101
2	**3**	Bi-[7]	2/30	~50	47	89
3	**5**	As-$[-]_{AP}$	2/6	7.5		
4	**6**	Bi-$[7]_P$				3
5	**7**	Bi-[5]			>100	89
6	**8**	Sb-[7]	7/12	>50	>100	26
7	**9**	Sb-$[7]_P$	0.7/1.7	3.2		3
8	**10**	Sb-[5]	5/23	>50	>100	90
9	**11**	Sb-[6]	9/26	>50	>100	54
10	**12**	Sb-[2.2.2]	10/36	>50		
11	**13**	As-$[7]_P$	1/6	3.9		
12	**14**	As-$[7]_{AP}$	5/9	5.6		
13	**15**	As-$[6]_{AP}$	0.6/4	19		

[a]Inhibitory activities of pnictogen-thiol compounds against the uptake of ETP transporter **21** and lentivectors. [b]Compounds, with the indication of pnictogen (Pn), ring size ([*x*]), and substituents (P, phenyl; AP, *para*-aminophenyl; A, acid); see Figure 2 for structures. [c]The concentrations needed to inhibit the uptake of ETP transporter **21** (10 μM) by 15/50% into HeLa Kyoto cells under co-incubation conditions. [d]The concentrations needed to reduce the cell viability by 50% under the conditions in *c*. [e]Relative entry of SARS-CoV-2 spike pseudo-lentiviral vector into A549 cells overexpressing ACE2 and TMPRSS2 in the presence of 10 μM inhibitors. [f]Viability of cells under the conditions in *e*.

and disulfides (Figure S2). The homologous dithiastibepane Sb-[7] **8** had an about 4 times weaker MIC = 7 μM, while the steeper dose response with co-incubation translated into a twice stronger IC_{50} = 12 μM (Table 1 and Figure S3). Toxicity was low up to 50 μM. The complementary dithiarsepane was not accessible because of the toxicity of the starting material.

Responding to the search of lentivector entry inhibition in the antimony series (*vide infra*), an unexchangeable phenyl in dithiastibepane Sb-$[7]_P$ **9** was considered to limit intramolecular O–Sb contacts to noncovalent pnictogen bonds and enforce ring-opening exchange cascades (Figure 1C). With MIC = 700 nM and IC_{50} = 1.7 μM, the phenylated dithiastibepane **9** was among the most potent inhibitors of the whole series but showed high toxicity (Figure 5C). Ring contraction to the minimalist dithiastibolane Sb-[5] **10** kept the MIC = 5 μM below the lead structure Sb-[7] **8**. The intermediate dithiastibinane Sb-[6] **11** was less active, possibly due to the inactivation of the antimony relay by intramolecular pnictogen bonding. The corresponding trithiastibabicyclooctane Sb-[2.2.2] **12**, a well-explored supramolecular chemistry motif operating with pnictogen bonds,[43] had almost the same, comparably weak MIC = 10 μM.

Permanent phenyl substituents also opened the door to arsenic relays. However, dithiarsepane As-$[7]_P$ **13**, the homologue of the most active Sb(III) **9**, was too toxic for meaningful inhibition experiments (Figure 5E). High toxicity found for As-$[-]_{AP}$ **5** was more surprising because it has been described early on as an inhibitor of HIV uptake.[37,38] Toward less toxic As(III) p-CAXs, the fusion of the aPAO and the DTT motif in As-$[7]_{AP}$ **14** was disappointing. With record MIC = 600 nM, ring contraction from arsepane As-$[7]_{AP}$ **14** to arsinane As-$[6]_{AP}$ **15** was more promising, but with RV_{50} = 19 μM, toxicity remained rather high.

The solution was to replace the alcohol in ring-contracted As-$[6]_{AP}$ **15** with an acid, that is to build the arsinane ring from

https://doi.org/10.1021/jacsau.2c00017
JACS Au 2022, 2, 1105–1114

asparagusic acid **1**. The resulting aPAO-AspA hybrid As-[6]$_{APA}$ **2** excelled with good activity (MIC = 6 μM, IC_{50} = 29 μM) and low toxicity up to 50 μM (Figure 5D,E). This finding was remarkable because the individual components were toxic (**5**) and inactive as inhibitors (**1**), respectively.[11] In As-[6]$_{APA}$ **2**, intra- and intermolecular pnictogen bonding and variable amine protonation were available to modulate the reactivity (Figure 3). This could, for instance, trigger thiolate exchange but prevent dithiol release from the arsenic relay with deepened σ holes and temporary covalent As−O bonds, respectively (Figure 4B), or account for selectivity (Figure 4C,D) during exchange cascades (Figure 1A,C, **IV**−**V**).

Inhibition of Lentivector Entry

The potential of new p-CAXs to inhibit viral entry was explored with a lentivirus expressing the SARS-CoV-2 spike protein with D614G mutation and coding for a luciferase reporter.[11] A549 human lung alveolar basal epithelium cells overexpressing ACE2 and TMPRSS2 were treated for 1 h with p-CAXs before incubation for 6 h with the lentivirus and a 3 day period for luciferase expression. Dithiabismepane Bi-[7] **3** at a concentration of 10 μM inhibited the expression by more than 50% (Figures 6A and 5F and Table 1). Even at 2 μM, 25% inhibition of SARS-CoV-2 lentivector uptake was observed (Figure 6A).

The bismuth control Bi-[7]$_P$ **6** was toxic, and Bi-[5] **7** promoted rather than inhibited lentivector uptake (Figure 6A and Table 1). Uptake activation was commonly observed at the onset of membrane damage, i.e., cytotoxicity, and not further pursued, although potential use for gene transfection is understood. The different behavior of controls **6** and **7** supported that the oxygen-bridged dithiabismepane scaffold of Bi-[7] **3** is essential to inhibit uptake; bismuth extraction by complete exchange with cellular thiols would equal out the activity of Bi-[7] **3** and Bi-[5] **7**. In **3**, the vicinal alcohols could serve to prevent such extraction by contributing temporarily covalent Bi−O bonds.

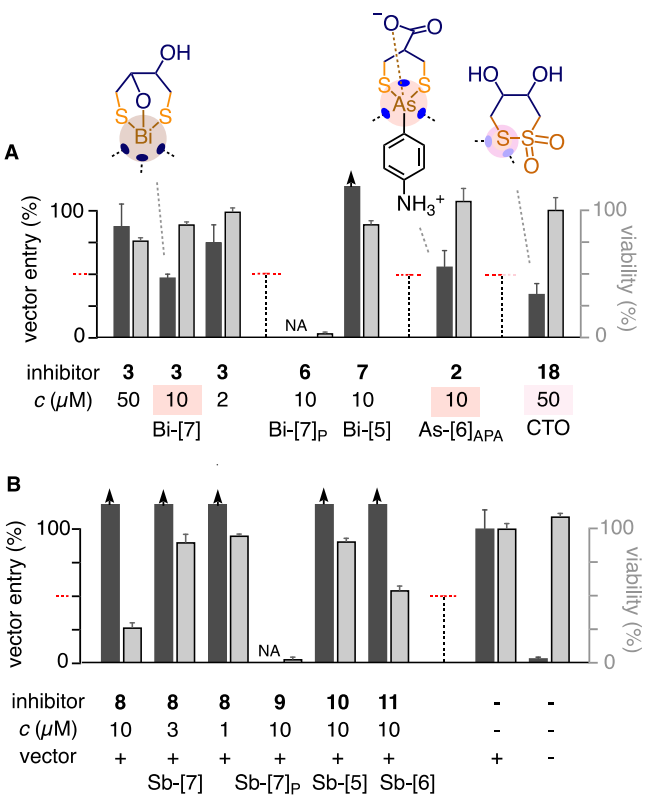

Figure 6. Normalized luminescence intensity (black) and viability (gray) for A549 human lung alveolar basal epithelium cells overexpressing ACE2 and TMPRSS2 after incubation with (A) Bi(III), As(III), and (B) Sb(III) inhibitor candidates and controls at concentrations *c* for 1 h, then with a lentivirus expressing the D614G SARS-CoV-2 spike protein and coding for luciferase for 6 h, followed by 3 days for luciferase expression (upward arrows: increase of uptake due, presumably, to the onset of toxicity). Experiments were performed in triplicate, error bars represent standard deviation.

Without bismuth, the DTT or DTE precursors fail to inhibit thiol-mediated uptake.[11] Their activation as cascade exchangers by oxidation to thiosulfonate **18** gave an $IC_{50} \approx 50$ μM and inactivity at 10 μM (Figure 6A).[11,60] The inhibition of SARS-CoV-2 lentivector uptake by CAX **18** was thus five times weaker compared to p-CAX **3** with $IC_{50} \approx 10$ μM. This comparison supported that the activation of cyclic disulfides by ring expansion with pnictogen relays is more powerful than activation by oxidation.

Moving from bismuth to arsenic, the only nontoxic inhibitor of the cytosolic delivery with transporter **21** was dithiarsinane **2** (Figure 5). Inhibition of SARS-CoV-2 lentivector uptake by this nontoxic arsenic relay As-[6]$_{APA}$ **2** was in the range of the bismuth relay Bi-[7] **3**, characterized by an $IC_{50} \sim 10$ μM (Figure 6A). This finding suggested that organocyclic As(III) relays are as promising as Bi(III) relays as long as toxicity is under control. We repeat that in As-[6]$_{APA}$ **2**, quite remarkably, this is realized by combining components that are either toxic (As-[-]$_{AP}$ **5**) or inactive (**1**) when separated, with coupled pnictogen bonding and amine protonation available to avoid excessive and achieve selective exchange cascades. It could also be argued that it is the carboxylate in As-[6]$_{APA}$ **2** that detoxifies As-[-]$_{AP}$ **5** because the negative charge hinders access to intracellular targets. This explanation would be supported by the persistently high toxicity of less hydrophilic analogues **13**−**15**. However, in the context of thiol-mediated uptake, the penetration of cells and the inhibition of cellular entry are considered as different expressions of the same dynamic covalent exchange cascades (Figure 1). The existence of good inhibitors that do not penetrate cells is thus unlikely, and the origin of the low toxicity of As-[6]$_{APA}$ **2** is related to unique selectivity and reactivity (Figures 3 and 4) rather than reduced cellular uptake. Efforts to use analogues of **2** for cytosolic delivery are ongoing and would be reported in due course.

Unlike bismuth and arsenic, antimony relays failed to inhibit lentivirus entry so far (Figure 6B). Sb-[7] **8**, the homologue of the best bismuth relay Bi-[7] **3**, was not much less potent as an inhibitor of the transporter **21** (Figure 5E) but only enhanced lentivirus uptake (Figure 6B). Presumably toxicity-related, uptake activation did not disappear even at 1 μM. Like the bismuth homologue Bi-[5] **7**, ring-contracted Sb-[6] **11** and Sb-[5] **10** were increasingly toxic activators (Figure 6).

Trends as for Sb-[7] **8** were found with the phenylated analogue Sb-[7]$_P$ **9**. This p-CAX was the most potent inhibitor of transporter **21** (Figure 5C,E) but as toxic as the bismuth homologue Bi-[7]$_P$ **6** in the lentivector uptake assay (Figure 6). The previously reported Sb(III) and Bi(III) pnictogen-bonding catalysts with three permanent 3,4,5-trifluorophenyl substituents[47] were also tested and found to be nontoxic but inactive as inhibitors of cytosolic uptake of transporter **21**, also in the presence of up to five equivalents of reduced asparagusic acid **1** as pnictogen-bonding counterpart of the activating motif in As-[6]$_{APA}$ **2** (not shown).

https://doi.org/10.1021/jacsau.2c00017
JACS Au 2022, 2, 1105−1114

CONCLUSIONS

In summary, the insertion of pnictogen relays to activate cyclic disulfide cascade exchangers has afforded a family of pnictogen-expanded cascade exchangers (p-CAXs). Two conceptually new lead motifs stand out. The bicyclic bismuth relay **3** and the phenylated arsenic relay **2** exhibit rich structural diversity (Figure 3) and dynamic covalent exchange cascades (Figure 4), and they inhibit both the thiol-mediated cytosolic delivery with a classical transporter (Figure 5) and the entry of SARS-CoV-2 lentivectors (Figure 6). Their potency exceeds the activity of the previous best, that is the cyclic thiosulfonate **18**, by nearly 1 order of magnitude. They are also much better than the popular ebselen,[61−63] which inhibits also both thiol-mediated cytosolic delivery with transporter **21** and the entry of SARS-CoV-2 lentivectors, but the latter only at high IC_{50} with high toxicity.[60] The availability of privileged scaffolds with and without permanent phenyl substituent on the pnictogen relay is important because they provide access to different cascade exchange chemistries (Figures 1C,D, 3, and 4). The availability of privileged scaffolds with As(III) and Bi(III) relays is attractive because their coordination chemistry covers two extremes that provide complementary characteristics in the dynamic covalent exchange cascades related to thiol-mediated uptake (Figure 4C,D). Namely, As(III) prefers the six-membered 1,3,2-dithiarsinane and Bi(III) the seven-membered 1,3,2-dithiabismepane rings. Exchange kinetics of these most stable rings supports the fact that lentivector entry inhibition coincides with exchange cascades that occur without the release of the pnictogen relay and involve important contributions from pnictogen bonds.

Future will tell whether the inhibition of the cytosolic delivery by thiol-mediated uptake and lentivector entry by one and the same dynamic covalent CAX is more than a coincidence. So far, bismuth- and antimony-centered antiviral candidates are mostly expected to inhibit proteases and other cysteine-rich proteins, often exhibiting multitarget activity but mostly without obvious involvement in the cellular entry.[27−29] However, the number of known CAXs capable to inhibit both the cytosolic delivery by thiol-mediated uptake and viral entry continues to increase with this study. Well-known for other viruses, particularly HIV,[1,38] the possibility of thiol-mediated uptake of SARS-CoV-2 has so far received little support. However, thiol-mediated processes have been considered,[39] and the number of receptors possibly involved in both continues to increase (transferrin receptor,[1,16,17] SCARB1,[1,15,17] PDIs,[38] integrins, etc). Thiol-mediated uptake thus increasingly emerges as complex circuitry that possibly encodes more generally for the entry into cells. Elucidation of this dynamic covalent multitarget network and the possible role of the here introduced pnictogen relays in this more general context is promising with regard to drug delivery and drug discovery, but exceptionally challenging.

EXPERIMENTAL METHODS

Materials

Pnictogen exchangers **3**,[25] **5**,[64] **8**,[25] **10**,[65] **12**,[43] **13**,[25] and **15**[66] and transporter **21**[58] were prepared by the reported procedures. Synthetic procedures and characterization of **2**, **6**, **7**, **9**, **11**, **14**, and **20** are given in the Supporting Information.

Computational Studies

Calculations were performed using the Gaussian 09 program (Rev. D01).[67] All structures were optimized using M06-2X/6-311++G** for light atoms (H, C, N, O, F, S, Cl) and aug-cc-pVTZ-PP for heavy atoms (As, Bi) in water solution, using the SMD model.[68] Frequency calculations were performed at the same level to confirm minima (no negative frequencies).

Pnictogen-Exchange Kinetics

Kinetics of fluorescence intensity change (λ_{ex} = 465 nm, λ_{em} = 555 nm) were monitored during the addition of **20** (0.1 μM), pnictogen inhibitors (**2**, **3**, **5**, **8**, **9**, **13**, **14**, **15**; 0.1 μM), and thiols (**4**, **16**, **17**, GSH, reduced BSA; various concentrations) in aqueous buffer (10 mM HEPES, 0.1 M NaCl, pH 7.4) containing TCEP (5 μM) at 25 °C.

High-Content High-Throughput Inhibitor Screening

Pre-Incubation Method. HeLa Kyoto cells were incubated with inhibitor solutions (various concentrations, duplicated) in FluoroBrite Dulbecco's modified Eagle's medium (DMEM) on a 96-well plate at 37 °C with 5% CO_2 for 1 h. The cells were then washed and incubated with transporter **21** (10 μM) in FluoroBrite DMEM for 30 min at 37 °C with 5% CO_2. The cells were then washed again and incubated with Hoechst 33342 (10 μg/L) and PI (1 μg/mL) in FluoroBrite DMEM for 15 min at 37 °C with 5% CO_2. The cells were washed and kept in clean FluoroBrite DMEM at 37 °C with 5% CO_2 for live cell imaging.

Co-Incubation Method. Similarly, HeLa Kyoto cells were incubated with inhibitors for 1 h and transporter **21** was added without the washing process. The rest of the procedures are identical to those of the pre-incubation method.

Imaging and Data Analyses. SDCM images of cells were acquired using an IXM-C automated microscope at 377/50 nm excitation filter and 477/60 nm emission filter for Hoechst 33342 (blue), 475/34 nm excitation filter, and 536/40 nm emission filter for transporter **21** (green), and 531/40 nm excitation filter and 593/40 nm emission filter for PI (red). The blue and red channel images were used to segment the cell bodies and detect dead cells. Then, integrated fluorescence intensity values of **21** per cell were extracted only of live cells, normalized, and analyzed using the Hill equation to give MIC, IC_{50}, and the Hill coefficient.[11]

Lentivector Entry Inhibition

Freshly prepared stock solutions of inhibitors in dimethyl sulfoxide (DMSO) (10, 50, or 500 mM) were diluted 1000 times with culture media to give each desired solution with 0.1% of DMSO. A549 cells were treated with these solutions for 1 h and then the lentivirus (see the Supporting Information) was added. After 6 h, the culture media containing both compounds and lentivirus was discarded and fresh culture media added. After 72 h, 10 μL of the culture media was sampled and mixed with 50 μL of PBS containing 4 μM of Coelentrazine (Apollo Scientific) and luminescence generated by the Gaussia luciferase reporter was measured. Cell viability was measured in parallel with cell counting kit WST8 (Sigma Aldrich).[11] Details for all procedures are given in the Supporting Information.

ASSOCIATED CONTENT

Supporting Information

The Supporting Information is available free of charge at https://pubs.acs.org/doi/10.1021/jacsau.2c00017.

Detailed experimental procedures, material and methods, compound synthesis and characterization, original ^{1}H and ^{13}C NMR spectra, fluorescence kinetics for cascade exchange, cell culture procedures, high-content high-throughput imaging procedures, dose−response curves for the inhibition of the cytosolic delivery of **21**, and lentivector entry inhibition procedures, and computational data (PDF)

X-ray crystallographic procedures and data (CCDC 2130143) (CIF)

https://doi.org/10.1021/jacsau.2c00017
JACS Au 2022, 2, 1105−1114

AUTHOR INFORMATION

Corresponding Author

Stefan Matile − *Department of Organic Chemistry, University of Geneva, 1211 Geneva, Switzerland;* orcid.org/0000-0002-8537-8349; Email: stefan.matile@unige.ch

Authors

Bumhee Lim − *Department of Organic Chemistry, University of Geneva, 1211 Geneva, Switzerland*

Takehiro Kato − *Department of Organic Chemistry, University of Geneva, 1211 Geneva, Switzerland*

Celine Besnard − *Department of Organic Chemistry, University of Geneva, 1211 Geneva, Switzerland;* orcid.org/0000-0001-5699-9675

Amalia I. Poblador Bahamonde − *Department of Organic Chemistry, University of Geneva, 1211 Geneva, Switzerland;* orcid.org/0000-0002-5266-914X

Naomi Sakai − *Department of Organic Chemistry, University of Geneva, 1211 Geneva, Switzerland;* orcid.org/0000-0002-9460-1944

Complete contact information is available at: https://pubs.acs.org/10.1021/jacsau.2c00017

Notes

The authors declare the following competing financial interest(s): The content of this manuscript is part of the patent application EP 21 15 8201.0.

ACKNOWLEDGMENTS

The authors thank L. Zong, Y. Cheng, A.-T. Pham, A. Gini, and F. Coelho for contributions to inhibitor synthesis, D. Moreau and S. Vossio for assistance, Neurix and the NMR, MS, and Bioimaging platforms for services, and the University of Geneva (including an Innogap grant), the National Centre for Competence in Research (NCCR) Chemical Biology, the NCCR Molecular Systems Engineering and the Swiss NSF for financial support (Excellence Grant 200020 204175; 51NF40-185898, 51NF40-182895). The pCG1_SCoV-2 plasmid encoding SARS-CoV-2 S-protein was provided by Stefan Pöhlmann (Deutsches Primatenzentrum, Leibniz-Institute for Primate Research, Göttingen).

REFERENCES

(1) Laurent, Q.; Martinent, R.; Lim, B.; Pham, A.-T.; Kato, T.; López-Andarias, J.; Sakai, N.; Matile, S. Thiol-Mediated Uptake. *JACS Au* **2021**, *1*, 710−728.

(2) Yang, W.; Liu, X.; Li, H.; Zhou, J.; Chen, S.; Wang, P.; Li, J.; Yang, H. Disulfide-Containing Molecular Sticker Assists Cellular Delivery of DNA Nanoassemblies by Bypassing Endocytosis. *CCS Chem.* **2021**, *3*, 1178−1186.

(3) Du, S.; Liew, S. S.; Li, L.; Yao, S. Q. Bypassing Endocytosis: Direct Cytosolic Delivery of Proteins. *J. Am. Chem. Soc.* **2018**, *140*, 15986−15996.

(4) Lu, J.; Wang, H.; Tian, Z.; Hou, Y.; Lu, H. Cryopolymerization of 1,2-Dithiolanes for the Facile and Reversible Grafting-from Synthesis of Protein−Polydisulfide Conjugates. *J. Am. Chem. Soc.* **2020**, *142*, 1217−1221.

(5) Meng, X.; Li, T.; Zhao, Y.; Wu, C. CXC-Mediated Cellular Uptake of Miniproteins: Forsaking "Arginine Magic". *ACS Chem. Biol.* **2018**, *13*, 3078−3086.

(6) Felber, J. G.; Zeisel, L.; Poczka, L.; Scholzen, K.; Busker, S.; Maier, M. S.; Theisen, U.; Brandstädter, C.; Becker, K.; Arnér, E. S. J.; Thorn-Seshold, J.; Thorn-Seshold, O. Selective, Modular Probes for Thioredoxins Enabled by Rational Tuning of a Unique Disulfide Structure Motif. *J. Am. Chem. Soc.* **2021**, *143*, 8791−8803.

(7) Guo, J.; Wan, T.; Li, B.; Pan, Q.; Xin, H.; Qiu, Y.; Ping, Y. Rational Design of Poly(disulfide)s as a Universal Platform for Delivery of CRISPR-Cas9 Machineries toward Therapeutic Genome Editing. *ACS Cent. Sci.* **2021**, *7*, 990−1000.

(8) Ulrich, S. Growing Prospects of Dynamic Covalent Chemistry in Delivery Applications. *Acc. Chem. Res.* **2019**, *52*, 510−519.

(9) Oupický, D.; Li, J. Bioreducible Polycations in Nucleic Acid Delivery: Past, Present, and Future Trends. *Macromol. Biosci.* **2014**, *14*, 908−922.

(10) Kohata, A.; Hashim, P. K.; Okuro, K.; Aida, T. Transferrin-Appended Nanocaplet for Transcellular siRNA Delivery into Deep Tissues. *J. Am. Chem. Soc.* **2019**, *141*, 2862−2866.

(11) Cheng, Y.; Pham, A.-T.; Kato, T.; Lim, B.; Moreau, D.; López-Andarias, J.; Zong, L.; Sakai, N.; Matile, S. Inhibitors of Thiol-Mediated Uptake. *Chem. Sci.* **2021**, *12*, 626−631.

(12) Laurent, Q.; Martinent, R.; Moreau, D.; Winssinger, N.; Sakai, N.; Matile, S. Oligonucleotide Phosphorothioates Enter Cells by Thiol-Mediated Uptake. *Angew. Chem., Int. Ed.* **2021**, *60*, 19102−19106.

(13) Crooke, S. T.; Seth, P. P.; Vickers, T. A.; Liang, X. The Interaction of Phosphorothioate-Containing RNA Targeted Drugs with Proteins Is a Critical Determinant of the Therapeutic Effects of These Agents. *J. Am. Chem. Soc.* **2020**, *142*, 14754−14771.

(14) Miller, C. M.; Donner, A. J.; Blank, E. E.; Egger, A. W.; Kellar, B. M.; Østergaard, M. E.; Seth, P. P.; Harris, E. N. Stabilin-1 and Stabilin-2 Are Specific Receptors for the Cellular Internalization of Phosphorothioate-Modified Antisense Oligonucleotides (ASOs) in the Liver. *Nucleic Acids Res.* **2016**, *44*, 2782−2794.

(15) Wei, C.; Wan, L.; Yan, Q.; Wang, X.; Zhang, J.; Yang, X.; Zhang, Y.; Fan, C.; Li, D.; Deng, Y.; Sun, J.; Gong, J.; Yang, X.; Wang, Y.; Wang, X.; Li, J.; Yang, H.; Li, H.; Zhang, Z.; Wang, R.; Du, P.; Zong, Y.; Yin, F.; Zhang, W.; Wang, N.; Peng, Y.; Lin, H.; Feng, J.; Qin, C.; Chen, W.; Gao, Q.; Zhang, R.; Cao, Y.; Zhong, H. HDL-Scavenger Receptor B Type 1 Facilitates SARS-CoV-2 Entry. *Nat. Metab.* **2020**, *2*, 1391−1400.

(16) Tang, X.; Yang, M.; Duan, Z.; Liao, Z.; Liu, L.; Cheng, R.; Fang, M.; Wang, G.; Liu, H.; Xu, J.; Kamau, P. M.; Zhang, Z.; Yang, L.; Zhao, X.; Peng, X.; Lai, R. Transferrin Receptor Is Another Receptor for SARS-CoV-2 Entry. *bioRxiv* **2020**, DOI: 10.1101/2020.10.23.350348.

(17) Abegg, D.; Gasparini, G.; Hoch, D. G.; Shuster, A.; Bartolami, E.; Matile, S.; Adibekian, A. Strained Cyclic Disulfides Enable Cellular Uptake by Reacting with the Transferrin Receptor. *J. Am. Chem. Soc.* **2017**, *139*, 231−238.

(18) Tombling, B. J.; Wang, C. K.; Craik, D. J. EGF-like and Other Disulfide-Rich Microdomains as Therapeutic Scaffolds. *Angew. Chem., Int. Ed.* **2020**, *59*, 11218−11232.

(19) Cantuti-Castelvetri, L.; Ojha, R.; Pedro, L. D.; Djannatian, M.; Franz, J.; Kuivanen, S.; van der Meer, F.; Kallio, K.; Kaya, T.; Anastasina, M.; Smura, T.; Levanov, L.; Szirovicza, L.; Tobi, A.; Kallio-Kokko, H.; Österlund, P.; Joensuu, M.; Meunier, F. A.; Butcher, S. J.; Winkler, M. S.; Mollenhauer, B.; Helenius, A.; Gokce, O.; Teesalu, T.; Hepojoki, J.; Vapalahti, O.; Stadelmann, C.; Balistreri, G.; Simons, M. Neuropilin-1 Facilitates SARS-CoV-2 Cell Entry and Infectivity. *Science* **2020**, *370*, 856−860.

(20) Karges, J.; Stokes, R. W.; Cohen, S. M. Metal Complexes for Therapeutic Applications. *Trends Chem.* **2021**, *3*, 523−534.

(21) Karges, J.; Cohen, S. M. Metal Complexes as Antiviral Agents for SARS-CoV-2. *ChemBioChem* **2021**, *22*, 2600−2607.

(22) Liu, C.; Shin, J.; Son, S.; Choe, Y.; Farokhzad, N.; Tang, Z.; Xiao, Y.; Kong, N.; Xie, T.; Kim, J. S.; Tao, W. Pnictogens in Medicinal Chemistry: Evolution from Erstwhile Drugs to Emerging Layered Photonic Nanomedicine. *Chem. Soc. Rev.* **2021**, *50*, 2260−2279.

(23) Duffin, R. N.; Werrett, M. V.; Andrews, P. C. Antimony and Bismuth as Antimicrobial Agents. In *Advances in Inorganic Chemistry*, Sadler, P. J.; van Eldik, R., Eds.; Academic Press, 2020; Vol. 75, pp 207−255.

(24) Lloyd, N. C.; Morgan, H. W.; Nicholson, B. K.; Ronimus, R. S. The Composition of Ehrlich's Salvarsan: Resolution of a Century-Old Debate. *Angew. Chem., Int. Ed.* **2005**, *44*, 941−944.
(25) Ioannou, P. V.; Tsivgoulis, G. M. The Reaction of Dithioerythritol and Dithiothreitol with As(III), Sb(III), and Bi(III) Compounds. *Monatsh. Chem.* **2015**, *146*, 249−257.
(26) Ioannou, P. V.; Tsivgoulis, G. M. Thiolates of Arsenic(III), Antimony(III), and Bismuth(III) with DL-α-Dihydrolipoic Acid. *Monatsh. Chem.* **2014**, *145*, 897−909.
(27) Voss, S.; Rademann, J.; Nitsche, C. Peptide-Bismuth Bicycles: In Situ Access to Stable Constrained Peptides with Superior Bioactivity. *Angew. Chem., Int. Ed.* **2022**, *61*, No. e202113857.
(28) Tao, X.; Zhang, L.; Du, L.; Liao, R.; Cai, H.; Lu, K.; Zhao, Z.; Xie, Y.; Wang, P.-H.; Pan, J.-A.; Zhang, Y.; Li, G.; Dai, J.; Mao, Z.-W.; Xia, W. Allosteric Inhibition of SARS-CoV-2 3CL Protease by Colloidal Bismuth Subcitrate. *Chem. Sci.* **2021**, *12*, 14098−14102.
(29) Wang, R.; Chan, J. F.-W.; Wang, S.; Li, H.; Zhao, J.; Ip, T. K.-Y.; Zuo, Z.; Yuen, K.-Y.; Yuan, S.; Sun, H. Orally Administered Bismuth Drug Together with *N*-Acetyl Cysteine as a Broad-Spectrum Anti-Coronavirus Cocktail Therapy. *Chem. Sci.* **2022**, *13*, 2238−2248.
(30) Reuther, J. F.; Dahlhauser, S. D.; Anslyn, E. V. Tunable Orthogonal Reversible Covalent (TORC) Bonds: Dynamic Chemical Control over Molecular Assembly. *Angew. Chem., Int. Ed.* **2019**, *58*, 74−85.
(31) Ayme, J.-F.; Dhers, S.; Lehn, J.-M. Triple Self-Sorting in Constitutional Dynamic Networks: Parallel Generation of Imine-Based CuI, FeII, and ZnII Complexes. *Angew. Chem., Int. Ed.* **2020**, *59*, 12484−12492.
(32) Phan, N.-M.; Percástegui, E. G.; Johnson, D. W. Dynamic Covalent Chemistry as a Facile Route to Unusual Main-Group Thiolate Assemblies and Disulfide Hoops and Cages. *ChemPlusChem* **2020**, *85*, 1270−1282.
(33) Collins, M. S.; Carnes, M. E.; Sather, A. C.; Berryman, O. B.; Zakharov, L. N.; Teat, S. J.; Johnson, D. W. Pnictogen-Directed Synthesis of Discrete Disulfide Macrocycles. *Chem. Commun.* **2013**, *49*, 6599−6601.
(34) Walker, A. S.; Rablen, P. R.; Schepartz, A. Rotamer-Restricted Fluorogenicity of the Bis-Arsenical ReAsH. *J. Am. Chem. Soc.* **2016**, *138*, 7143−7150.
(35) Griffin, B. A.; Adams, S. R.; Tsien, R. Y. Specific Covalent Labeling of Recombinant Protein Molecules Inside Live Cells. *Science* **1998**, *281*, 269−272.
(36) Pulcu, G. S.; Mikhailova, E.; Choi, L.-S.; Bayley, H. Continuous Observation of the Stochastic Motion of an Individual Small-Molecule Walker. *Nat. Nanotechnol.* **2015**, *10*, 76−83.
(37) Gallina, A.; Hanley, T. M.; Mandel, R.; Trahey, M.; Broder, C. C.; Viglianti, G. A.; Ryser, H. J.-P. Inhibitors of Protein-Disulfide Isomerase Prevent Cleavage of Disulfide Bonds in Receptor-Bound Glycoprotein 120 and Prevent HIV-1 Entry. *J. Biol. Chem.* **2002**, *277*, 50579−50588.
(38) Ryser, H. J.-P.; Flückiger, R. Keynote Review: Progress in Targeting HIV-1 Entry. *Drug Discovery Today* **2005**, *10*, 1085−1094.
(39) Koppisetti, R. K.; Fulcher, Y. G.; Van Doren, S. R. Fusion Peptide of SARS-CoV-2 Spike Rearranges into a Wedge Inserted in Bilayered Micelles. *J. Am. Chem. Soc.* **2021**, *143*, 13205−13211.
(40) Deprey, K.; Kritzer, J. A. HaloTag Forms an Intramolecular Disulfide. *Bioconjugate Chem.* **2021**, *32*, 964−970.
(41) Scheiner, S. The Pnicogen Bond: Its Relation to Hydrogen, Halogen, and Other Noncovalent Bonds. *Acc. Chem. Res.* **2013**, *46*, 280−288.
(42) Bauzá, A.; Mooibroek, T. J.; Frontera, A. The Bright Future of Unconventional σ/π-Hole Interactions. *ChemPhysChem* **2015**, *16*, 2496−2517.
(43) Moaven, S.; Watson, B. T.; Thompson, S. B.; Lyons, V. J.; Unruh, D. K.; Casadonte, D. J.; Pappas, D.; Cozzolino, A. F. Self-Assembly of Reversed Bilayer Vesicles through Pnictogen Bonding: Water-Stable Supramolecular Nanocontainers for Organic Solvents. *Chem. Sci.* **2020**, *11*, 4374−4380.
(44) Humeniuk, H. V.; Gini, A.; Hao, X.; Coelho, F.; Sakai, N.; Matile, S. Pnictogen-Bonding Catalysis and Transport Combined: Polyether Transporters Made in Situ. *JACS Au* **2021**, *1*, 1588−1593.
(45) Park, G.; Brock, D. J.; Pellois, J.-P.; Gabbaï, F. P. Heavy Pnictogenium Cations as Transmembrane Anion Transporters in Vesicles and Erythrocytes. *Chem* **2019**, *5*, 2215−2227.
(46) Breugst, M.; Koenig, J. J. σ-Hole Interactions in Catalysis. *Eur. J. Org. Chem.* **2020**, *2020*, 5473−5487.
(47) Gini, A.; Paraja, M.; Galmés, B.; Besnard, C.; Poblador-Bahamonde, A. I.; Sakai, N.; Frontera, A.; Matile, S. Pnictogen-Bonding Catalysis: Brevetoxin-Type Polyether Cyclizations. *Chem. Sci.* **2020**, *11*, 7086−7091.
(48) Yang, M.; Tofan, D.; Chen, C.-H.; Jack, K. M.; Gabbaï, F. P. Digging the Sigma-Hole of Organoantimony Lewis Acids by Oxidation. *Angew. Chem., Int. Ed.* **2018**, *57*, 13868−13872.
(49) Zhang, J.; Wei, J.; Ding, W.-Y.; Li, S.; Xiang, S.-H.; Tan, B. Asymmetric Pnictogen-Bonding Catalysis: Transfer Hydrogenation by a Chiral Antimony(V) Cation/Anion Pair. *J. Am. Chem. Soc.* **2021**, *143*, 6382−6387.
(50) Wang, F.; Planas, O.; Cornella, J. Bi(I)-Catalyzed Transfer-Hydrogenation with Ammonia-Borane. *J. Am. Chem. Soc.* **2019**, *141*, 4235−4240.
(51) Scilabra, P.; Terraneo, G.; Resnati, G. The Chalcogen Bond in Crystalline Solids: A World Parallel to Halogen Bond. *Acc. Chem. Res.* **2019**, *52*, 1313−1324.
(52) Biot, N.; Bonifazi, D. Chalcogen-Bond Driven Molecular Recognition at Work. *Coord. Chem. Rev.* **2020**, *413*, No. 213243.
(53) Vogel, L.; Wonner, P.; Huber, S. M. Chalcogen Bonding: An Overview. *Angew. Chem., Int. Ed.* **2019**, *58*, 1880−1891.
(54) Bickerton, L. E.; Docker, A.; Sterling, A. J.; Kuhn, H.; Duarte, F.; Beer, P. D.; Langton, M. J. Highly Active Halogen Bonding and Chalcogen Bonding Chloride Transporters with Non-Protonophoric Activity. *Chem. - Eur. J.* **2021**, *27*, 11738−11745.
(55) Gleiter, R.; Haberhauer, G.; Werz, D. B.; Rominger, F.; Bleiholder, C. From Noncovalent Chalcogen−Chalcogen Interactions to Supramolecular Aggregates: Experiments and Calculations. *Chem. Rev.* **2018**, *118*, 2010−2041.
(56) Shybeka, I.; Aster, A.; Cheng, Y.; Sakai, N.; Frontera, A.; Vauthey, E.; Matile, S. Naphthalenediimides with Cyclic Oligochalcogenides in Their Core. *Chem. - Eur. J.* **2020**, *26*, 14059−14063.
(57) Mantina, M.; Chamberlin, A. C.; Valero, R.; Cramer, C. J.; Truhlar, D. G. Consistent van der Waals Radii for the Whole Main Group. *J. Phys. Chem. A* **2009**, *113*, 5806−5812.
(58) Zong, L.; Bartolami, E.; Abegg, D.; Adibekian, A.; Sakai, N.; Matile, S. Epidithiodiketopiperazines: Strain-Promoted Thiol-Mediated Cellular Uptake at the Highest Tension. *ACS Cent. Sci.* **2017**, *3*, 449−453.
(59) Lim, B.; Cheng, Y.; Kato, T.; Pham, A.-T.; Le Du, E.; Mishra, A. K.; Grinhagena, E.; Moreau, D.; Sakai, N.; Waser, J.; Matile, S. Inhibition of Thiol-Mediated Uptake with Irreversible Covalent Inhibitors. *Helv. Chim. Acta* **2021**, *104*, No. e2100085.
(60) Kato, T.; Lim, B.; Anh, A.-T.; Poblador-Bahamonde, A. I.; Moreau, D.; Sakai, N.; Matile, S. Cyclic Thiosulfonates for Thiol-Mediated Uptake: Cascade Exchangers, Transporters, Inhibitors *JACS Au* 2022, *2*, DOI: 10.1021/jacsau.1c00573.
(61) Jin, Z.; Du, X.; Xu, Y.; Deng, Y.; Liu, M.; Zhao, Y.; Zhang, B.; Li, X.; Zhang, L.; Peng, C.; Duan, Y.; Yu, J.; Wang, L.; Yang, K.; Liu, F.; Jiang, R.; Yang, X.; You, T.; Liu, X.; Yang, X.; Bai, F.; Liu, H.; Liu, X.; Guddat, L. W.; Xu, W.; Xiao, G.; Qin, C.; Shi, Z.; Jiang, H.; Rao, Z.; Yang, H. Structure of Mpro from SARS-CoV-2 and Discovery of Its Inhibitors. *Nature* **2020**, *582*, 289−293.
(62) Sargsyan, K.; Lin, C.-C.; Chen, T.; Grauffel, C.; Chen, Y.-P.; Yang, W.-Z.; Yuan, H.; Lim, C. Multi-Targeting of Functional Cysteines in Multiple Conserved SARS-CoV-2 Domains by Clinically Safe Zn-Ejectors. *Chem. Sci.* **2020**, *11*, 9904−9909.
(63) Sies, H.; Parnham, M. J. Potential Therapeutic Use of Ebselen for COVID-19 and Other Respiratory Viral Infections. *Free Radicals Biol. Med.* **2020**, *156*, 107−112.

(64) He, Y.; Shin, J.; Gong, W.; Das, P.; Qu, J.; Yang, Z.; Liu, W.; Kang, C.; Qu, J.; Kim, J. S. Dual-Functional Fluorescent Molecular Rotor for Endoplasmic Reticulum Microviscosity Imaging during Reticulophagy. *Chem. Commun.* **2019**, *55*, 2453−2456.
(65) Zhihua, L.; Shaowu, D. Nonlinear Optical Crystal 2-Pyridyl Thioethanedithiol Antimony and its Preparation Method and Application. CN Patent CN1017473792010.
(66) Hu, G.; Jia, H.; Hou, Y.; Han, X.; Gan, L.; Si, J.; Cho, D.-H.; Zhang, H.; Fang, J. Decrease of Protein Vicinal Dithiols in Parkinsonism Disclosed by a Monoarsenical Fluorescent Probe. *Anal. Chem.* **2020**, *92*, 4371−4378.
(67) Frisch, M. J.; Trucks, G. W.; Schlegel, H. B.; Scuseria, G. E.; Robb, M. A.; Cheeseman, J. R.; Scalmani, G.; Barone, V.; Mennucci, B.; Petersson, G. A.; Nakatsuji, H.; Caricato, M.; Li, X.; Hratchian, H. P.; Izmaylov, A. F.; Bloino, J.; Zheng, G.; Sonnenberg, J. L.; Hada, M.; Ehara, M.; Toyota, K.; Fukuda, R.; Hasegawa, J.; Ishida, M.; Nakajima, T.; Honda, Y.; Kitao, O.; Nakai, H.; Vreven, T.; Montgomery, J. A., Jr.; Peralta, J. E.; Ogliaro, F.; Bearpark, M.; Heyd, J. J.; Brothers, E.; Kudin, K. N.; Staroverov, V. N.; Kobayashi, R.; Normand, J.; Raghavachari, K.; Rendell, A.; Burant, J. C.; Iyengar, S. S.; Tomasi, J.; Cossi, M.; Rega, N.; Millam, J. M.; Klene, M.; Knox, J. E.; Cross, J. B.; Bakken, V.; Adamo, C.; Jaramillo, J.; Gomperts, R.; Stratmann, R. E.; Yazyev, O.; Austin, A. J.; Cammi, R.; Pomelli, C.; Ochterski, J. W.; Martin, R. L.; Morokuma, K.; Zakrzewski, V. G.; Voth, G. A.; Salvador, P.; Dannenberg, J. J.; Dapprich, S.; Daniels, A. D.; Farkas, Ö.; Foresman, J. B.; Ortiz, J. V.; Cioslowski, J.; Fox, D. J. *Gaussian 09*, Revision D.01; Gaussian, Inc.: Wallingford CT, 2009.
(68) Marenich, A. V.; Cramer, C. J.; Truhlar, D. G. Universal Solvation Model Based on Solute Electron Density and on a Continuum Model of the Solvent Defined by the Bulk Dielectric Constant and Atomic Surface Tensions. *J. Phys. Chem. B* **2009**, *113*, 6378−6396.

https://doi.org/10.1021/jacsau.2c00017
JACS Au 2022, 2, 1105−1114